Bio-Design and Manufacturing (2025) 8:917–929
https://doi.org/10.1631/bdm.2500211

RESEARCH ARTICLE

A microneedle substrate-based sutureless engineered cardiac patch for myocardial infarction repair

Zibo Liu[1,2,3] · Pengcheng Yang[1,2,3] · Yueming Tian[1,2,3] · Heyuan Deng[1,2,3] · Jingjing Xia[1,2,3] · Binhan Li[1,2,3] · Bingyan Wu[1,2,3] · Yongcong Fang[1,2,3] · Zhuo Xiong[1,2,3] · Ting Zhang[1,2,3,4]

Received: 29 April 2025 / Accepted: 27 July 2025

Abstract

Myocardial infarction (MI) is a challenging condition that results in scar formation on the ventricular wall, causing myocardial damage and ventricular thinning. Engineered cardiac patches (ECPs) designed to regenerate myocardial tissue have been proposed to repair the ventricular wall and replenish myocardial cells. However, their clinical use is limited by manufacturing and fixation challenges. This study introduces a manufacturing strategy for a composite ECP, which comprises an antiadhesion shell layer, a conductive myocardial tissue, and an exosome-laden microneedle substrate. The ECP can anchor to the infarcted myocardium through its microneedle substrate. Meanwhile, its outer shell prevents nonspecific adhesion, enabling stable and suture-free attachment. Using this microneedle substrate, we applied a 3D-printed ECP in a rat model of post-MI repair. Our results showed that this strategy reduced left ventricular damage, improved cardiac ejection fraction, decreased the fibrotic area, increased ventricular wall thickness, improved microvascular recovery, and thus facilitated the repair of maladaptive ventricular remodeling post-MI. This microneedle substrate holds great promise for use in the fixation of patches during the repair of myocardial tissue and other organs, thereby promoting the clinical application of tissue-engineered patches.

Graphical abstract

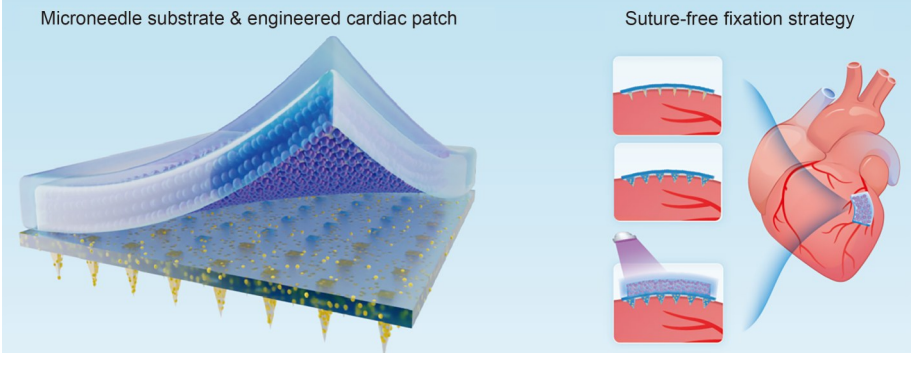

Keywords Microneedles · Engineered cardiac patches · Myocardial infarction repair

✉ Zhuo Xiong
xiongzhuo@tsinghua.edu.cn

✉ Ting Zhang
t-zhang@mail.tsinghua.edu.cn

[1] Biomanufacturing Center, Department of Mechanical Engineering, Tsinghua University, Beijing 100084, China

[2] Biomanufacturing and Rapid Forming Technology Key Laboratory of Beijing, Beijing 100084, China

[3] "Biomanufacturing and Engineering Living Systems" Innovation International Talents Base (111 Base), Beijing 100084, China

[4] State Key Laboratory of Tribology in Advanced Equipment, Tsinghua University, Beijing 100084, China

1 Introduction

Myocardial infarction (MI) is a common cardiovascular disease that, due to the challenges in curing it, results in a significant number of young deaths each year. Thrombolytic drugs are primarily used for treatment in the early stages of acute MI. Nevertheless, after local myocardial cell death following an acute infarction, scar tissue forms, and the surrounding myocardial cells are overloaded, causing further cell death [1]. Consequently, the scar tissue expands, resulting in overall thinning of the ventricular wall. In recent years, engineered cardiac patches (ECPs) have received increasing attention as a promising regenerative therapeutic approach for the treatment of MI [2, 3].

ECPs are conventionally secured to the damaged myocardium by suturing [4, 5]. Although sutures provide firm mechanical fixation, they can interrupt perfusion within the patch, cause bleeding, injure the surrounding healthy tissue, and elevate the risk of infection [6, 7]. Such additional trauma may further impair left ventricular function and enlarge the injury area. Some researchers have constructed myocardial patches in situ at the infarct site using crosslinking strategies [8–10]. For instance, Liang et al. synthesized a biocompatible, sprayable conductive hydrogel via Fe^{3+}-initiated in situ polymerization of pyrrole and dopamine, which crosslinks on the epicardial surface to form an ECP [11]. In recent years, microneedle-integrated patches have also been investigated for MI repair, yielding promising therapeutic outcomes [12, 13]. Their unique structure confers various advantages in terms of excellent adhesion properties and drug delivery capabilities. Researchers have demonstrated that drug-loaded microneedle patches, carrying growth factors, microRNAs, and exosomes, can effectively improve myocardial remodeling and fibrosis post-MI, thereby enhancing cardiac function [14–16].

Nonetheless, ECPs fabricated via in situ crosslinking or microneedle-based strategies are formed under physicochemical conditions that living cardiomyocytes cannot tolerate, thereby preventing cell incorporation and limiting the potential of ECPs for true myocardial regeneration [17, 18]. Taken together, the conflict between the need for suture-free fixation and cardiomyocyte loading in ECPs represents a major challenge that restricts their reparative efficacy and clinical translation. In this study, we address the above-mentioned limitations through an in situ photopolymerization strategy that combines a microneedle substrate with cell-laden ECPs to achieve suture-free fixation. An exosome-encapsulated microneedle substrate (GPMN*) was fabricated from a gelatin-methacryloyl (GelMA) prepolymer doped with poly(3,4-ethylenedioxythiophene):polystyrene sulfonate (PEDOT:PSS). In practice, the dried GPMN* is first anchored to the infarcted myocardium, and then a cardiomyocyte-laden ECP is placed on its outer surface. Ultraviolet (UV) irradiation triggers rapid photopolymerization, forming a stable composite patch that is firmly attached without sutures.

To further evaluate the therapeutic potential of the microneedle substrate combined with a cell-laden ECP (Fig. 1),

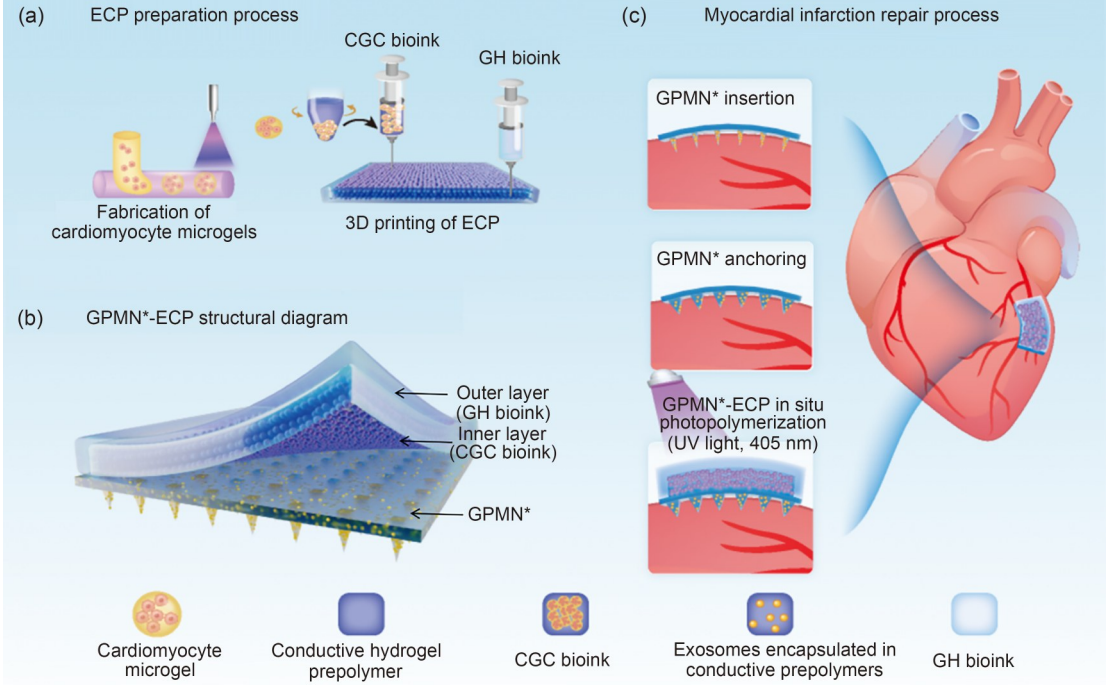

Fig. 1 Schematic of the GPMN*-ECP strategy. (a) ECP preparation process. (b) GPMN*-ECP structural diagram. (c) Myocardial infarction repair process. CGC: conductive granular composite; GH: GelMA/methacrylated hyaluronic acid (HAMA)

we used a previously reported conductive granular composite bioink (CGC bioink) to 3D-print an ECP for implantation in a rat MI model [4]. The resulting ECP featured a bilayer architecture: (i) an inner cardiomyocyte-like layer printed with a CGC bioink and (ii) an outer protective layer printed with a GelMA/methacrylated hyaluronic acid (HAMA) bioink (GH bioink). In vivo studies have demonstrated that compared to the suture-fixed ECP, the assembled GPMN*-ECP significantly improved angiogenesis and myogenesis, attenuated fibrotic remodeling, and improved overall cardiac function, highlighting its efficacy for post-infarction repair. Hence, this microneedle substrate provides a versatile, suture-free anchoring platform for ECPs and demonstrates promising potential for broader applications in the repair of other tissues and organs.

2 Materials and methods

2.1 Materials

GelMA (EFL-GelMA-90) and HAMA (EFL-HAMA-150K) were purchased from EFL-Tech (Suzhou) Co., Ltd., China. The aqueous solution of PEDOT:PSS (Clevios PH1000) was purchased from Heraeus (Germany). Cardiac troponin T (c-TnT, 1:200, ab8295), gap junction protein connexin 43 (Cx43, 1:200, ab11370), mannose receptor (CD206, 1:200, ab64693), von Willebrand factor (vWF, 1:200, ab11713), goat anti-mouse immunoglobulin G (IgG) H&L (Alexa Fluor® 488, ab150113), goat anti-rabbit IgG H&L (Alexa Fluor® 594, ab150080) antibodies, and the enzyme-linked immunosorbent assay (ELISA) kits for interleukin (IL)-1β and IL-10 were acquired from Abcam (Cambridge, UK). The antibody for α-smooth muscle actin (α-SMA, 67735-1) was obtained from Proteintech Group (Wuhan, China). Human umbilical mesenchymal stem cell exosomes (MSC-exos, E939302) were purchased from Maclin (Shanghai, China).

2.2 Cell culture

Neonatal rat cardiomyocytes (NRCMs) were isolated from neonatal rat hearts. Briefly, the ventricular tissue was extracted, cut into approximately 1-mm^3 pieces, and digested overnight at 4 °C on a rocking platform in a 0.05% (0.5 g/L) trypsin solution without ethylenediamine tetraacetic acid (EDTA). Moreover, myocardial tissues were enzymatically digested using 1 mg/mL type II collagenase (Worthington Biochemical Corporation, Lakewood, New Jersey, USA) until a single-cell suspension was obtained. The resulting cells were collected, filtered through a 100-μm cell strainer, and centrifuged at 1200 r/min for 3 min. The isolated cells were then seeded into tissue culture flasks and incubated for 1 h to allow differential adhesion. Subsequently, nonadherent NRCMs were collected for further experiments.

Human umbilical vein endothelial cells (HUVECs) were purchased from the American Type Culture Collection (ATCC, CRL-1730) and cultured in endothelial cell growth medium (EGM)-2 obtained from Lonza Group Ltd. (Catalog No. CC-3126, Basel, Switzerland). Human monocytes (THP-1) were purchased from Wuhan Pricella Biotechnology Co., Ltd. (China) and cultured using matching complete media. The THP-1 cells were differentiated into macrophages by treating them with 10 ng/mL phorbol 12-myristate 13-acetate (PMA; Cat. No. abs9107, Absin, Shanghai, China) for 24 h.

2.3 Preparation of hydrogel prepolymers and bioinks

GelMA and HAMA prepolymers were prepared using the respective commercial kits following the manufacturers' instructions. The required amount of hydrogel was added to phosphate-buffered saline (PBS) solution containing 0.5% lithium phenyl-2,4,6-trimethylbenzoylphosphinate and incubated in a 37 °C water bath for 20 min to obtain the desired concentration. The GelMA/PEDOT:PSS conductive hydrogel prepolymer (GP prepolymer) was prepared by mixing 7.5% GelMA prepolymer with 1% PEDOT:PSS solution in a 10:1 ratio. The mixture was then filtered through a 0.22-μm sterile filter to remove any undissolved precipitates and aggregated particles.

The CGC bioink was prepared using a previously described method [4], combining myocardial microgels with conductive hydrogel prepolymers. An L-shaped polydimethylsiloxane (PDMS) microfluidic chip with a 600-μm inner diameter was used for bioink preparation. Briefly, a copper wire matching the diameter of the microchannel was embedded into the groove of a resin mold. PDMS (Sylgard 184, Dow Corning Corporation, Midland, Michigan, USA) was then cast into the mold and cured at 70 °C. After curing, the copper wire was carefully extracted to form the channel, and the resulting L-shaped PDMS chip was demolded for use. Then, 3% GelMA prepolymer containing 5×10^7 NRCMs/mL was introduced from one inlet (with a flow rate of 2 mL/h), and mineral oil with 2% (volume fraction) Span 80 was injected in the other inlet (with a flow rate of 15 mL/h). Then, a catheter was used to connect the outlet of the microfluidic chip to a centrifuge tube placed in an ice-water bath to collect the microgels. Next, the microgels (in mineral oil) were photocrosslinked under 405-nm UV light at an intensity of 30 mW/cm^2 for 30 s. PBS was then added to the centrifuge tube, and the suspension was gently triturated with a Pasteur pipette to wash the microgels. After centrifugation at 800 r/min for 3 min, the

microgels were pelleted at the bottom of the tube, and the supernatant, containing the mineral oil and excess PBS, was carefully removed (Fig. S1a in the supplementary information). This washing process was repeated three to five times until the mineral oil was almost completely removed. An excess amount of GP prepolymer (one to two times the volume of the precipitated microgel) was added to the centrifuge tube. The precipitated microgel was vortexed to ensure thorough mixing and then centrifuged again at 800 r/min. Next, the excess GP prepolymer was removed from the upper layer (Fig. S1b in the supplementary information). This process was repeated three to five times to replace the PBS within the gaps between the microgels with the GP prepolymer, resulting in the formation of CGC bioink (with a microgel solid content of 60.38% (mass fraction)).

The GH bioink was formulated by combining 7.5% GelMA and 7.5% HAMA in a 1:1 ratio, after preincubation in a 37 °C water bath.

2.4 Bioprinting of ECPs

The ECP featured a bilayer structure, fabricated using two different bioinks. The outer layer, with a box-like structure and a thickness of approximately 300 μm, was printed using the GH bioink. The inner layer, encapsulating cardiomyocytes, was printed using the CGC bioink and had a thickness of approximately 550 μm. Bioprinting was performed using a dual-head 3D bioprinter (Biomaker 2i, Sunp Bio-Tech, China). The optimized printing parameters for the two bioinks were as follows:

GH bioink: 25 G needle, extrusion rate of 0.5 mL/min, printing speed of 5 mm/s, line spacing of 0.5 mm, layer height of 0.2 mm, and printing temperature of 20 °C.

CGC bioink: 20 G needle, extrusion rate of 2 mL/min, printing speed of 5 mm/s, line spacing of 1 mm, layer height of 0.4 mm, and printing temperature of 20 °C.

After printing, the ECPs were exposed to UV light (30 mW/cm^2) for 30 s for curing. They were then cultured in Dulbecco's modified Eagle medium (DMEM; Thermo Fisher, USA) supplemented with 2% fetal bovine serum (FBS; Biological Industries, Israel), 1% penicillin-streptomycin (Life Technologies, USA), and 1% nonessential amino acids (NEAA; Life Technologies).

2.5 Immunostaining

The ECPs, macrophages, and cardiac tissue sections were fixed in 4% paraformaldehyde (PFA) for 20 min and then washed with PBS. For fluorescence imaging, the samples were permeabilized with 0.1% (mass fraction) Triton X-100 at room temperature for 30 min. After blocking with 10% (mass fraction) goat serum at 37 °C for 30 min, the samples were incubated overnight at 4 °C with primary antibodies (c-TnT and Cx43). After three washes with PBS, the samples were incubated with the corresponding fluorophore-conjugated secondary antibodies for 2 h at room temperature in the dark. Finally, the cell nuclei were stained with 4′,6′-diamidino-2-phenylindole (DAPI), placed in a confocal-specific petri dish, and observed under a laser scanning confocal microscope (FV3000, Olympus, Tokyo, Japan).

2.6 Preparation of the GelMA/PEDOT:PSS microneedles (GPMNs)

The GelMA/PEDOT:PSS microneedles (GPMNs) were fabricated using a PDMS micromold, with microneedle lengths of 500, 700, and 1000 μm (GPMN-500, GPMN-700, and GPMN-1000, respectively). The microneedles were tetrahedral in shape, with the base length equal to half the needle length. The needle tips in the mold were spaced 800 μm apart, and the needle cavities were arranged in a 14×14 array. During the experiment, the GP prepolymer was added to the mold cavities, and the mold was centrifuged at 1500 r/min for 3 min to remove air from the conical microneedle cavities. Then, GPMN-500, GPMN-700, and GPMN-1000 molds were obtained by drying in a 37 °C oven. All samples were examined under a field emission-scanning electron microscope (FE-SEM; GeminiSEM 300, Zeiss, Germany). GPMN* was prepared as described previously, with exosomes incorporated into the GP prepolymer, which was then placed into the GPMN-700 mold and shaped following the same procedure.

2.7 Mechanical characterization

All mechanical tests were conducted using a mechanical test instrument (Bose ElectroForce 3200, Bose Corporation, Eden Prairie, USA). At least six samples were tested for each condition. Before all measurements, the samples were measured using a vernier caliper to determine their actual sizes.

The compression mechanical properties were evaluated by 3D printing CGC bioink and GH bioink into cylindrical samples with a diameter of 8 mm and a height of 5 mm. The samples were then compressed at a rate of 0.1 mm/s until rupture. The elastic modulus was calculated using the elastic region (5%–20% strain) of the stress–strain curve. Similarly, tensile measurements were performed using a uniaxial stretch test, with samples stretched to 50% strain. The CGC samples and GH samples were fabricated as single-layer constructs, with a length of 25 mm and a width of 5 mm, using their respective bioinks. The bilayered ECPs were printed with the same dimensions (length: 25 mm; width: 5 mm). The elastic modulus was calculated from the elastic region (5%–20% strain) of the stress–strain curve.

The obtained GPMNs (with the tips facing upward) were placed on the ElectroForce instrument. The force sensor gradually approached the GPMN patch at a speed of 0.1 mm/s. The measurement began when the sensor made contact with the tips and ended either when the sensor descended by 0.4 mm or when the microneedles fractured. The tensile strength and lap shear strength of the GPMNs were tested after in situ crosslinking with hydrogel patches of the same size (composed of 7.5% GelMA containing red dye). Porcine myocardial and hydrogel patches were first adhered to glass slides using a cyanoacrylate adhesive, and then the slides were fixed to the mechanical test instrument. The displacement speed was set at 0.1 mm/s, and the maximum values from the stress–strain curve were used to calculate the tensile strength and lap shear strength.

2.8 Hematoxylin and eosin (H&E) staining of GPMNs

After fixing the GPMNs on the surface of the porcine heart, the punctured tissue sections were harvested and fixed in 4% PFA at 4 °C for 24 h. The sections were then dehydrated through a graded ethanol series, washed using xylene, and embedded in paraffin. After deparaffinization and rehydration, the sections were stained with hematoxylin for 5 min, rinsed in running tap water, differentiated in 1% acid alcohol, and stained blue with saturated lithium carbonate solution. Next, the sections were counterstained with eosin for 2 min, dehydrated through a graded ethanol series, washed using xylene, shifted to microscope slides, and covered with coverslips using a resinous mounting medium.

2.9 In vitro co-culture of GPMN*

A wound scratch model was used to evaluate cell migration. Briefly, HUVECs were seeded in 6-well transwell plates and cultured until they reached near confluence. A scratch was made in each group using a 200-μL pipette tip, and cell debris was subsequently removed. GPMN* samples with exosome concentrations of 10^8 mL^{-1} and 10^9 mL^{-1} were added to the upper chambers (pore size: 80 μm; Falcon, Corning Incorporated, Corning, New York, USA). After wetting the GPMN* in the culture medium, they were crosslinked under UV light (30 mW/cm^2, 20 s) and placed into the corresponding groups, with six replicates per group. In the control group, GPMN-700 without exosomes was placed in the upper chamber. HUVECs in all groups were imaged using a microscope-mounted camera at 0 and 12 h after scratching. The wound closure rate was quantified using the ImageJ software.

Similarly, macrophages (THP-1 cells induced with PMA as described in Sect. 2.2) were counted and seeded in 6-well transwell plates at a density of 10^6 cells/well. GPMN* samples with varying exosome concentrations were placed in the upper chambers and crosslinked. After 24 h of incubation, macrophages adhering to the well bottoms were subjected to CD206 immunostaining, and the supernatants were collected for ELISA. The ELISA was performed according to the manufacturer's instructions. Standard solutions for each kit were prepared as per the manufacturer's instructions, and both the standard solutions and cell supernatants were dispensed into the wells, with appropriate replicates arranged. The wells were then washed three times with the wash solution and incubated with tetramethylbenzidine at room temperature for 10 min. After adding the stop solution, the analysis was immediately performed using a microplate reader at 450 nm.

2.10 Animal experiments

Sprague–Dawley rats (all males, approximately 8 weeks old) were obtained and divided into the following four groups: sham surgery group (Sham), MI group, ECP group, and GPMN*-ECP group, with eight rats in each group. The rats were anesthetized with isoflurane and put on mechanical ventilation. A 6-0 polypropylene suture was used to ligate the proximal left anterior descending (LAD) artery until a pale white area appeared in the left ventricle. The Sham group underwent the same thoracotomy procedure, but without ligating the LAD artery. To match the size of the rat heart, 8 mm×8 mm patches were printed for subsequent experiments. In the ECP group, the patches were sutured to the infarct area using 6-0 polypropylene sutures. In the GPMN*-ECP group, GPMN* was trimmed to match the size of the patch and inserted into the lateral wall of the left ventricle, followed by fixation of the patch using an in situ crosslinking method. To induce immunosuppression, the rats received daily subcutaneous injections of methylprednisolone (2 mg/kg) and azathioprine (2 mg/kg) post-surgery.

2.11 Evaluation of cardiac function

Echocardiography (Vevo2100, Visual Sonic, USA) was performed to evaluate left ventricular function in rats four weeks after patch transplantation. Following anesthesia, the rats' chests were shaved, and the animals were secured on the detection board. Key echocardiographic parameters, including ejection fraction (EF), fractional shortening (FS), left ventricular internal dimension in systole (LVIDs), and LVID in diastole (LVIDd), were analyzed to evaluate cardiac function.

2.12 Histological analysis

After four weeks of myocardial patch transplantation, the rats were anesthetized and euthanized via cervical

dislocation to harvest their hearts. Heart samples were preserved in optimal cutting temperature (OCT) compound, cryoprocessed, dehydrated through a graded ethanol series, embedded in paraffin, and sectioned at a thickness of 5 μm. The sections were stained with Masson's trichrome stain, and the infarct area and left ventricular wall thickness were measured under a microscope. The proportion of fibrosis area in the infarct zone was quantified using the ImageJ software.

2.13 Statistical analysis

All values were expressed as mean±standard deviation. Statistical differences between two sample groups were evaluated using Student's *t*-test, and one-way analysis of variance (ANOVA) was used to compare three sample groups. The significance levels were defined as $p<0.05$.

3 Results and discussion

3.1 Formulation and characterization of ECP

We designed a bilayered ECP with dimensions of 15 mm×15 mm. The inner layer consisted of a conductive myocardial tissue encapsulating the heart muscle, and the outer layer served as a protective shell with improved mechanical strength. The ECP was fabricated using two types of bioprinting inks (GH and CGC bioinks) through 3D printing. The CGC bioink, used for printing the inner conductive myocardium-like layer, is a conductive, cell-laden bioprinting ink based on a granular composite hydrogel, as previously reported by our group [4, 19]. To prepare CGC bioink, functionalized cardiomyocyte microgels were prepared by encapsulating cardiomyocytes in a low-concentration GelMA precursor using a microfluidic device. These microgels were then mixed with a high-concentration GelMA precursor containing PEDOT:PSS to obtain CGC bioink. In our previous study, we demonstrated that the conductive extracellular matrix possesses an electrical conductivity ((0.0031±0.00 018) S/cm) comparable to that of native myocardium and supports high post-printing cell viability ((76.1±4.89)% for C2C12 cells) [4]. The GH bioink, used for printing the outer layer of ECP, comprised a mixture of GelMA and HAMA precursors. GelMA is a commonly used material for bioprinting inks and has thermosensitive properties and photopolymerization capabilities essential for bio-3D printing [20]. HAMA hydrogels do not naturally contain arginine-glycine-aspartic acid (RGD) sequences, because hyaluronic acid (HA) is a nonadhesive glycosaminoglycan, and it is therefore often used in antiadhesion applications [21, 22]. Hence, the high-strength hydrogel shell printed using GH bioink not only increased the overall mechanical strength of the ECP and protected the internal cardiomyocyte-like tissue but also helped prevent undesired adhesion between the ECP and surrounding tissues.

As depicted in Fig. 2a, the filament diameters of GH and CGC bioinks were approximately 308.2 and 553.0 μm, respectively. We used a dual-head printer to fabricate the ECP within a culture dish. As illustrated in Fig. 2b, a single-layer shell was first printed using GH bioink, and then a layer of conductive, cell-laden cardiomyocyte-like tissue was printed inside the shell using CGC bioink. The vertical cross-section of ECP shown in Fig. S2 (supplementary information) reveals the bilayer structure that we designed. The compressive elastic modulus of the two inks was evaluated post-printing (Fig. 2c). The GH cylinder exhibited a higher elastic modulus than the CGC cylinder (84.8 kPa vs. 32.2 kPa). The overall tensile strength of the double-layer composite ECP was 46.6 kPa, which was higher than the tensile strength of the CGC layer alone (35.9 kPa), indicating the enhanced mechanical strength and protection conferred by the GH shell layer (Fig. 2d). We cultured the printed ECPs in vitro (Fig. 2e), where the cardiomyocytes were distributed within the microgel of the conductive myocardial layer. After one week of in vitro culture, immunofluorescence staining was performed with c-TnT (green) and Cx43 (red). As illustrated in Fig. 2f and Movie S1 (supplementary information), the network-like distribution of c-TnT and the expression of Cx43 in the intercellular spaces indicated that the NRCMs within the ECPs were highly mature. Figure S3 (supplementary information) shows a magnified view of a single cardiomyocyte microgel. Our previous studies showed that the microgel exerts a protective effect on NRCMs, alleviating the shear-induced damage during the printing process [4, 19]. Moreover, the conductive extracellular matrix of the CGC bioink promotes the survival, proliferation, maturation, and functional performance of NRCMs. In the present study, we used a multihead printing technique to construct composite ECPs with enhanced mechanical strength using a stronger hydrogel to protect the internal myocardial-like layer. The bilayer design helps prevent damage to the ECP before and after transplantation and ensures better mechanical support and protection for the MI region.

3.2 Synthesis and characterization of GPMN*

During the implantation and fixation of ECPs, the suturing process can cause damage to the myocardium. Some patches with microneedle structures have been applied in MI repair because of their ability to fix to the myocardial surface in a minimally invasive manner [14, 16, 23]. We designed a microneedle substrate using GelMA/PEDOT:PSS hydrogel precursors, specifically for securing the ECP. We

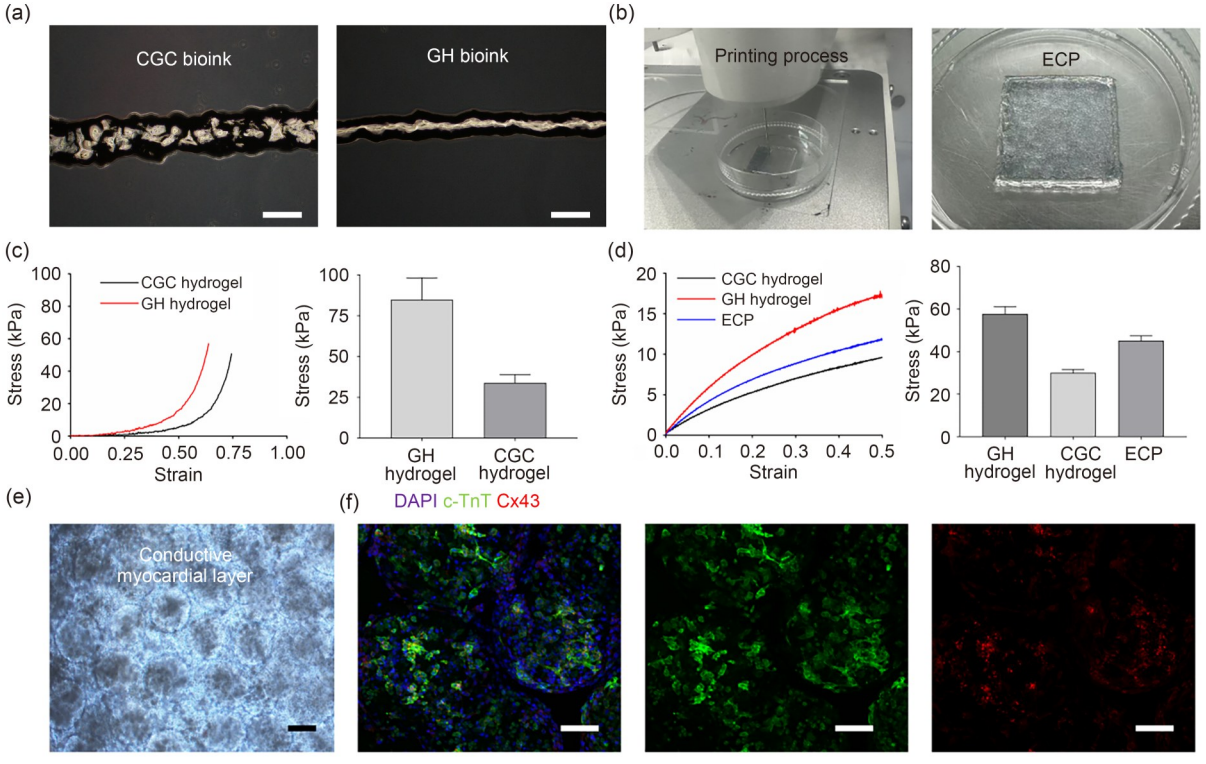

Fig. 2 Preparation and characterization of ECP. (a) CGC and GH bioinks. (b) ECP printing process and formation schematic. (c) Compressive elastic modulus of GH and CGC bioinks. (d) Mechanical properties of ECP. (e) Conductive myocardial layer of ECP. (f) Immunostaining of c-TnT (green) and Cx43 (red) proteins in ECPs. All data are expressed as mean±standard deviation (n=6). Scale bars are 500 μm in (a), 200 μm in (e), and 100 μm in (f)

selected GelMA/PEDOT:PSS hydrogel as the ideal material for the GPMNs because of its excellent biocompatibility, bioactivity, and electrical conductivity. Three types of microneedle array substrates were fabricated, each containing a 14×14 array with needle lengths of 500, 700, and 1000 μm, separately. As depicted in Fig. 3a, the GelMA/PEDOT:PSS prepolymer was introduced into the corresponding PDMS template and dried to obtain GPMN-500, GPMN-700, and GPMN-1000. We explored the mechanical strength of the GPMNs by placing different types of GPMNs, arranged in a 196-square array, horizontally. The displacement and force curves for each needle were recorded (Fig. 3b). The fracture forces of individual microneedles for GPMN-500, GPMN-700, and GPMN-1000 were 0.15, 0.35, and 0.69 N, respectively, indicating that the strength of the microneedles increased with size. The microstructure of GPMNs was also characterized (Figs. 3c and 3d). All GPMN tips were arranged in an array, with the microneedles exhibiting a tetrahedral shape, where the base edge length was half the needle length, and the tip-to-tip distance was 800 μm, as confirmed by SEM. We also measured the actual lengths of the microneedles, which were (433.8±24.3), (629.3±13.5), and (917.0±23.9) μm for GPMN-500, GPMN-700, and GPMN-1000, respectively (Fig. S4 in the supplementary information). We separately inserted three different microneedle substrates into the epicardial surface of porcine hearts. After insertion, all the microneedle substrates absorbed water and expanded, adhering to the myocardium (Fig. 3e). Longitudinal sections of porcine hearts with the fixed microneedle substrates were prepared and stained with H&E to observe the fixation effect of the microneedle substrates (Fig. 3f). We observed that the depth of penetration into the myocardial tissue gradually increased with increasing microneedle length, indicating a stronger fixation strength of longer microneedles.

Based on the aforementioned GPMNs, we proposed an in situ crosslinking strategy for the fixation of ECPs. As illustrated in Fig. 4a and Movie S2 (supplementary information), the crosslinking approach involved three major steps. First, the microneedle substrate was fixed onto the surface of the heart. Then, the ECP was placed on top of the microneedle substrate. Finally, the patch was crosslinked by exposure to UV light at a wavelength of 405 nm (30 mW/cm^2, 20 s). To further evaluate the fixation efficacy of this crosslinked patch, we investigated the tensile strength and lap shear strength of the hydrogel fixed onto the surface of the porcine heart. We used three different GPMNs with varying needle lengths to fix hydrogel patches of the same size (7.5% GelMA with red dye). As demonstrated in Figs. 4b and 4c, the tensile strength and the lap shear strength of the

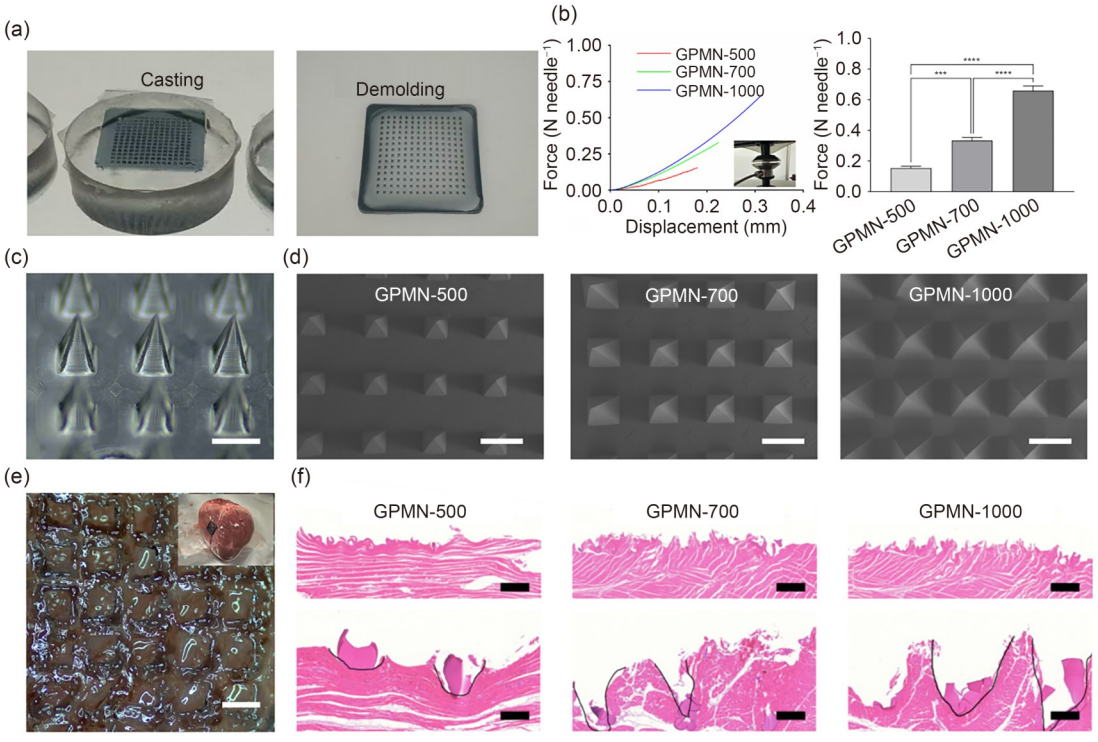

Fig. 3 Preparation and characterization of GPMNs. (a) GPMN formation process. (b) Compressive strength of GPMNs of different sizes. (c, d) GPMN morphology. (e) Schematic of GPMN fixation on the outer side of the porcine ventricular wall. (f) H&E staining after GPMN fixation. All data are expressed as mean±standard deviation (n=6). $^{***}p<0.001$ and $^{****}p<0.0001$. Scale bars are 500 μm in (c, d), 800 μm in (e), 1 mm in (f, top), and 200 μm in (f, bottom)

hydrogel patch increased with increasing needle length. The maximum tensile stress values corresponding to GPMN-500, GPMN-700, and GPMN-1000 were 2.6, 5.8, and 11.1 kPa, respectively, and the maximum lap shear strength values were 9.32, 16.31, and 24.76 kPa, respectively. We observed the fracture surfaces under an optical microscope (Fig. S5 in the supplementary information). In the GPMN-500 group, fracture primarily occurred at the microneedle-tissue interface. In contrast, in the GPMN-1000 group, fracture occurred almost entirely within the hydrogel (with the fracture surfaces predominantly composed of red-stained hydrogel). This finding indicated that when the microneedle length reached 1000 μm, the in situ crosslinking interface strength significantly surpassed that of the 7.5% GelMA hydrogel (approaching the strength of the ECP patch). Therefore, we used GPMN-700s in subsequent in vitro and in vivo analyses for further investigation.

Due to their excellent angiogenic and anti-inflammatory bioactivities, MSC-exos have been demonstrated to possess therapeutic value for MI repair [24, 25]. To further improve the repair effect of our devised patch, we incorporated MSC-exos at varying concentrations (10^8 mL^{-1} and 10^9 mL^{-1}) into the GP hydrogel used to fabricate the GPMN*. As shown in Fig. 4d, GPMN* was placed in a transwell and crosslinked to test its effects on endothelial cells and macrophages. A group of GPMN-700s without exosomes was also placed in the transwell and crosslinked as the control group. Endothelial cell migration was evaluated using a scratch assay in the co-culture system. After 12 h of co-culture, the presence of GPMN* significantly promoted wound closure (Fig. 4e). Compared to the control group (45.89%), the 10^8 mL^{-1} and 10^9 mL^{-1} groups exhibited higher healing rates (58.34% and 63.88%, respectively). The endothelial scratch assay showed that endothelial cells exposed to exosomes within the GPMN exhibited markedly increased migratory capacity, indicating the proangiogenic activity of the material [26]. Hence, the GPMN*-ECP strategy may promote revascularization and restore blood flow in the MI region. MSC-exos are capable of inducing macrophage phenotype polarization and have been widely applied in tissue injury and repair. We investigated the anti-inflammatory effects of GPMN* on PMA-treated THP-1 cells. After 1 d of co-culture, we conducted CD206 staining on THP-1 cells. We observed that GPMN* promoted the expression of CD206 inside the cells, indicating that the exosomes in the microneedle substrate regulated macrophage polarization, facilitating the transition from M1 to M2 phenotype (Fig. 4f). Next, we used ELISA to measure the concentrations of classical M1/M2 phenotype markers, interleukin-1 beta (IL-1β) and interleukin-10 (IL-10), in the supernatant (Fig. 4g). We observed a decrease in IL-1β concentration and a significant increase

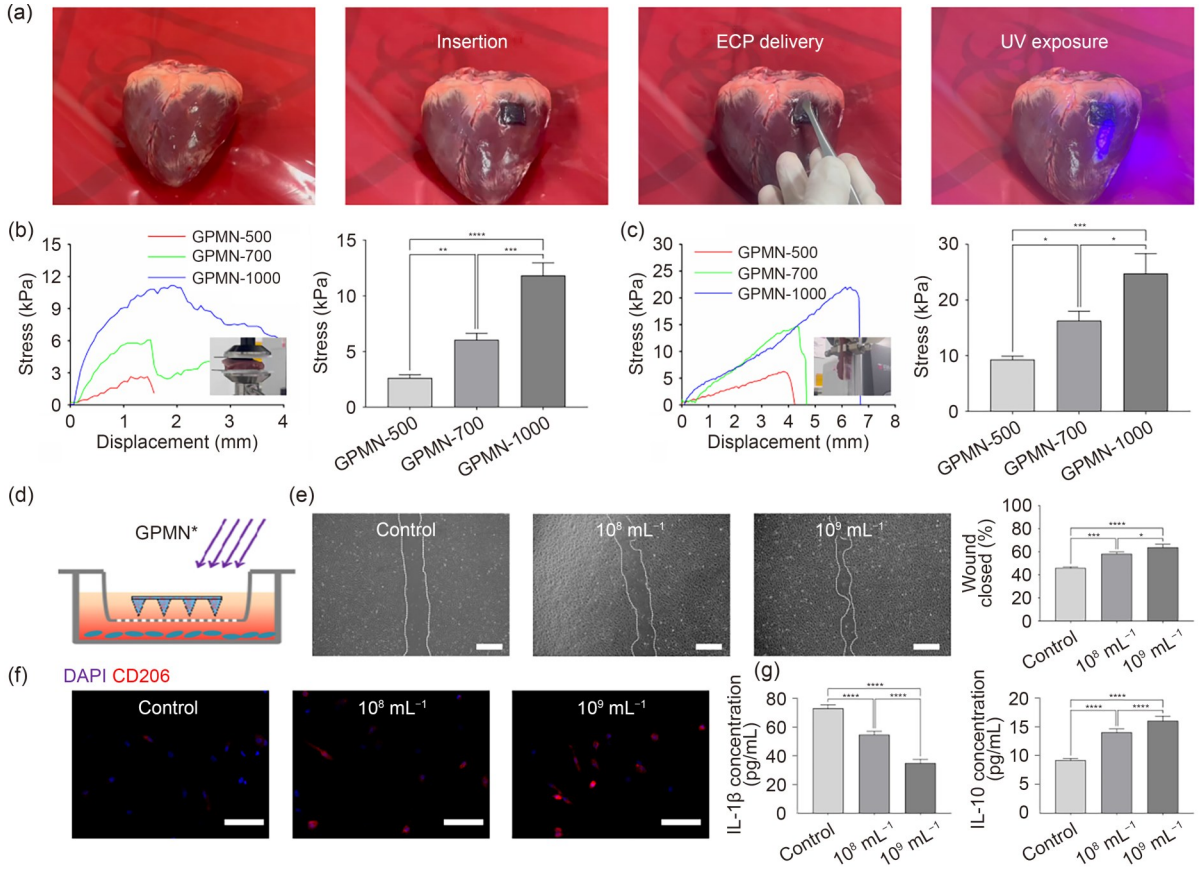

Fig. 4 GPMN*-ECP fixation strength characterization and in vitro biological characterization. (a) Schematic of the GPMN* -ECP strategy. (b) Tensile strength. (c) Lap shear strength. (d) GPMN* co-culture schematic. (e) Representative images of scratch wounds and quantitative analysis of the scratch assay (after 12 h of co-culture). (f) Macrophage immunofluorescence staining. (g) IL-1β/IL-10 ELISA results. All data are expressed as mean±standard deviation (n=6). $^{*}p<0.05$, $^{**}p<0.01$, $^{***}p<0.001$, and $^{****}p<0.0001$. Scale bars are 500 μm in (e) and 50 μm in (f)

in IL-10 concentration in the co-culture system. This result suggested a reduction in the M1 macrophage phenotype and an increase in the M2 macrophage phenotype, which was consistent with the findings from immunostaining.

In summary, this GPMN* -ECP approach can serve to shape the microneedles and fix the ECPs in place. Compared to the traditional methods, where microneedles are prepared through exposure and then dried, our approach avoided defects such as warping and shrinkage of the microneedle substrate after drying (Fig. S6 in the supplementary). In vitro experiments demonstrated that the microneedles can effectively fix the GelMA patch onto the surface of porcine hearts. GPMN* exhibited favorable biological functions, including proangiogenic and anti-inflammatory effects, which eventually attenuated the adverse post-MI cardiac remodeling.

3.3 Repair effects of GPMN*-ECP in rat MI models

We conducted further in vivo studies to explore the therapeutic effects of GPMN*-ECP in MI hearts. We investigated the feasibility, safety, and in vivo function of the GPMN*-ECP repair strategy using a rat MI model, which was generated by permanent ligation of the LAD coronary artery. The animals were divided into four experimental groups (Sham, MI, ECP, and GPMN* -ECP) and were followed for four weeks to allow cardiac remodeling.

The typical echocardiographic parameters of rats, including EF, FS, LVIDs, and LVIDd, were analyzed to assess the cardiac function of the rats after four weeks of treatment (Fig. 5a). Compared to the MI group, the reductions in EF and FS, as well as the increases in LVIDd and LVIDs, were effectively suppressed in the ECP and GPMN*-ECP groups (Fig. 5b). Furthermore, compared to the ECP group, the GPMN* -ECP group demonstrated a more pronounced reduction in LV chamber size, inhibition of LV remodeling, and reparation of LV function. Cardiac morphology was evaluated after four weeks by Masson's trichrome staining (Fig. 5c). Compared to the Sham group, the MI group exhibited significant collagen deposition and ventricular wall thinning in the infarcted area, whereas the region implanted with the hydrogel exhibited more myocardial tissue. Quantitative analysis indicated that both experimental groups

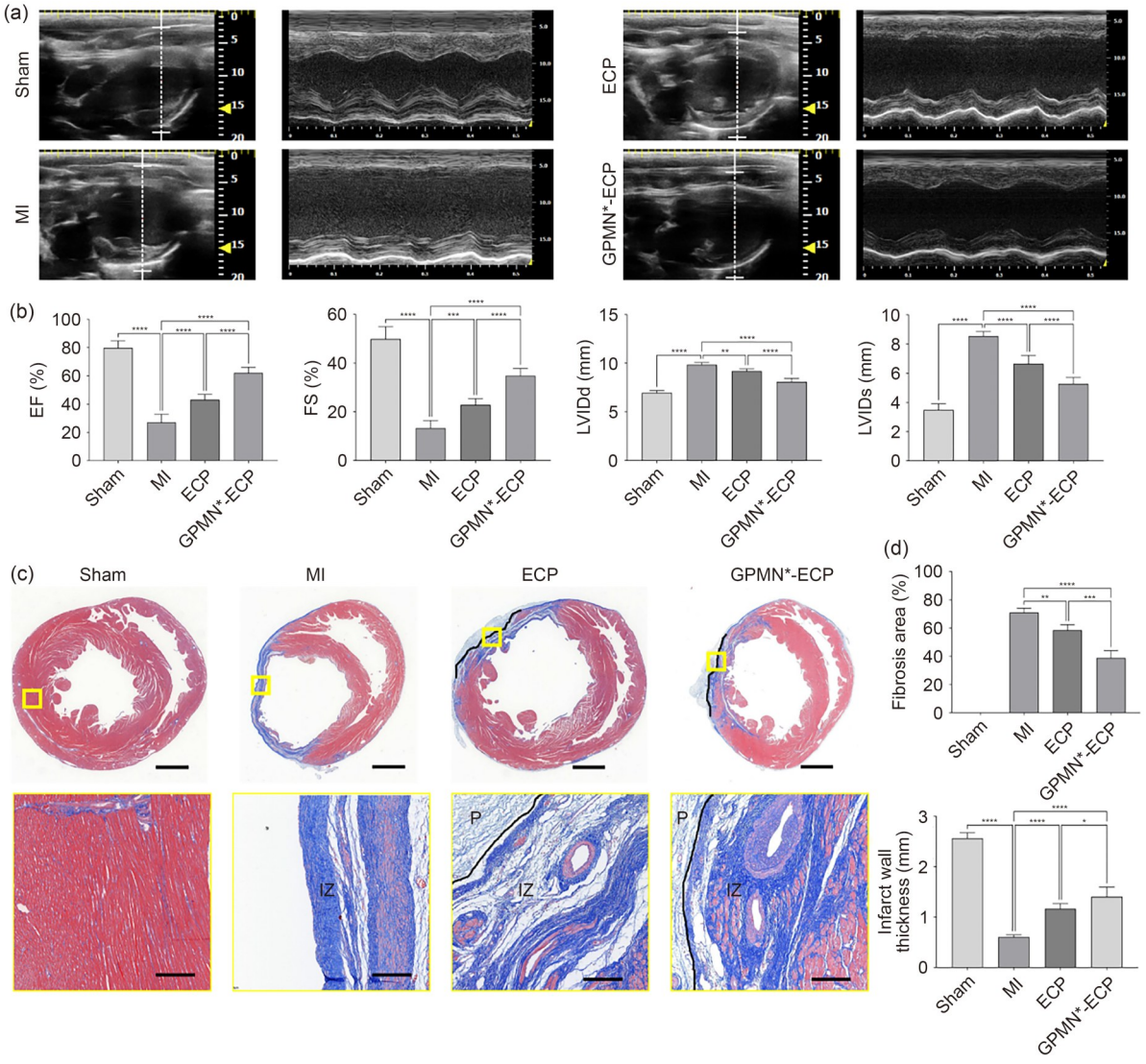

Fig. 5 Cardiac function and morphology at four weeks post-transplantation. (a) Representative echocardiographic images of hearts. (b) Quantitative comparisons of left ventricular function parameters in each group. (c) Masson's trichrome staining of rat heart tissue (IZ: infarct zone; P: patch). (d) Fibrosis area and infarct wall thickness in each group based on Masson's trichrome staining. Data are expressed as mean±standard deviation (n=6). $^{*}p<0.05$, $^{**}p<0.01$, $^{***}p<0.001$, and $^{****}p<0.0001$. Scale bars are 2.5 mm in (c, top) and 200 μm in (c, bottom)

using ECP repair showed significant reductions in the infarct area, with the GPMN*-ECP group exhibiting the smallest infarct size (Fig. 5d). The fibrotic area proportions in the ECP and GPMN*-ECP groups were (58.41±3.56)% and (38.76±4.71)%, respectively. Similarly, among the four groups, the GPMN*-ECP group exhibited the greatest left ventricular wall thickness ((1.40±0.17) mm).

The survival rate of cardiomyocytes in the infarcted area and the preservation of gap junctions between viable cardiomyocytes were evaluated by immunofluorescence staining using c-TnT and Cx43 (Figs. 6a and 6b). Compared to the MI and ECP groups, c-TnT and Cx43 were significantly upregulated in the GPMN*-ECP group, indicating a higher survival rate of cardiomyocytes and improved electrical and contractile function in this group post-treatment. Since restoration of blood supply to the infarcted area can rescue residual cardiomyocytes, we performed immunostaining with vWF and α-SMA to label microvessels and arterioles, respectively, to evaluate angiogenesis in the infarcted region (Figs. 6c and 6d). The GPMN*-ECP group demonstrated well-defined microvessel and arteriole structures in the infarcted area, with a significantly higher vessel density compared to the MI and ECP groups (Fig. 6e). Moreover, the GPMN*-ECP group exhibited larger vessel diameters than the ECP group. These findings might be attributed to the proangiogenic effects of exosomes contained within GPMN*.

In summary, the GPMN*-ECP strategy reduced surgical trauma, representing a simpler and more effective alternative to suturing. This strategy utilizes the minimally invasive fixation properties of the microneedles, resulting in better

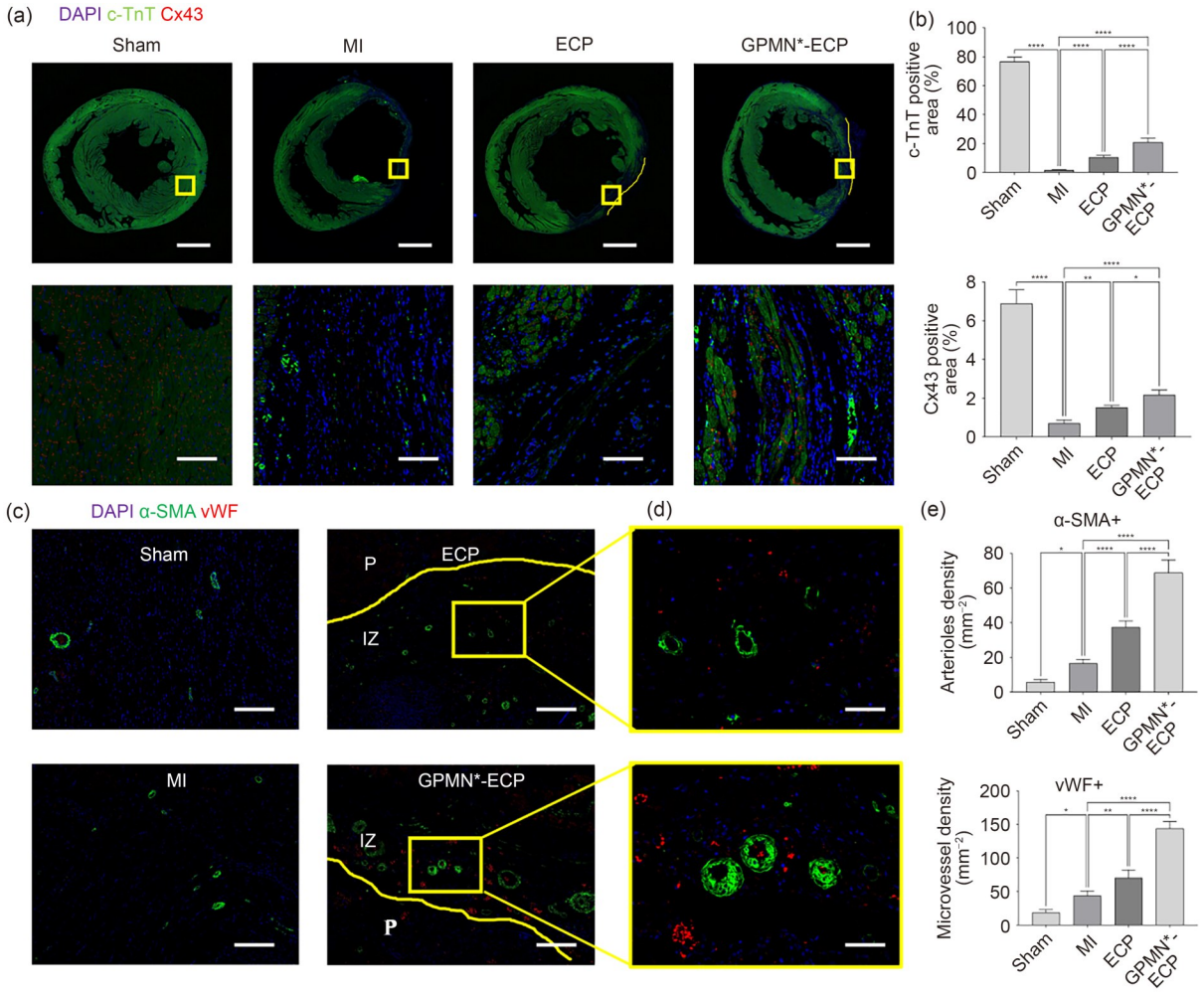

Fig. 6 Myocardial viability and revascularization in the infarcted heart at four weeks post-treatment. (a) Immunofluorescence staining with c-TnT and Cx43 in the heart sections of each group. (b) Quantitative expression area of c-TnT- and Cx43-positive area in the infarcted areas of different groups. (c, d) Immunofluorescence staining of rat hearts with α-SMA and vWF (IZ: infarct zone; P: patch). (e) Quantitative expression area of α-SMA and vWF in the infarcted areas of different groups. Data are expressed as mean±standard deviation (n=6). $^{*}p<0.05$, $^{**}p<0.01$, and $^{****}p<0.0001$. Scale bars are 2.5 mm in (a, top), 100 μm in (a, bottom), 200 μm in (c), and 50 μm in (d)

repair outcomes in the ECP-based myocardial regeneration approach. We believe that the GPMN*-ECP strategy holds promise for improved clinical application prospects. In this study, the primary material of the patch was GelMA, which is derived from animal-sourced gelatin. Although GelMA is commonly considered to have good biocompatibility and low immunogenicity in tissue engineering and regenerative medicine, it might induce immune reactions in sensitive individuals. Therefore, in practical applications, this patch may need to be used in combination with various immunosuppressive drugs. Furthermore, the bonding between ECP and GPMN* primarily relies on light-induced in situ crosslinking of hydrogel prepolymers, which imposes specific requirements on the material properties of ECP. ECP is manufactured using a light-curable hydrogel, and the residual acrylamide groups within ECP can further crosslink with GPMN*, thereby improving the adhesion strength at the interface. If ECP is used as a hydrogel crosslinked by enzymes or ions, it would be necessary to introduce photocrosslinkable double bonds into the material (such as alginate methacrylate or hyaluronic acid methacrylate) to ensure sufficient curing strength of the microneedle substrate. This study also focused on the fixation strength of three different types of microneedle substrates. In practical applications, the required fixation strength of ECP on the heart surface still requires further exploration to optimize the size and structure of microneedle substrates.

4 Conclusions

This study presents a composite myocardial patch comprising a 3D-printed ECP and a drug-loaded microneedle substrate for MI treatment. The ECP featured a dual-layer

patch structure fabricated by 3D printing, with the inner layer comprising a cardiomyocyte-like conductive layer encapsulating cardiomyocytes and the outer layer comprising a high-strength hydrogel, thereby improving the overall mechanical properties of the patch. This GPMN* substrate, prepared using a microneedle penetration fixation combined with an in situ crosslinking strategy, anchors the ECP to the epicardial surface of the heart, thereby eliminating the need for sutures that could cause additional tissue trauma. Furthermore, animal experiments demonstrated that, after transplantation, the infarct area was significantly reduced, neovascularization was increased, and cardiac function was improved. Therefore, this study proposes an effective strategy for MI repair based on the microneedle in situ crosslinking transplantation of ECP and offers a novel fixation approach for the repair of patches in other tissues and organs.

Supplementary Information The online version contains supplementary material available at https://doi.org/10.1631/bdm.2500211.

Acknowledgements This work was supported by the Beijing Natural Science Foundation (Nos. 7252285 and L246001), the National Natural Science Foundation of China (Nos. U21A20394 and 52305314), and the National Key Research and Development Program of China (No. 2023YFB4605800).

Author contributions Conceptualization, ZBL, ZX, and TZ; formal analysis, ZBL, PCY, and YMT; investigation, ZBL; methodology, ZBL, YMT, BYW, HYD, JJX, BHL, and YCF; writing—original draft, ZBL; writing—review & editing, ZBL, PCY, and TZ.

Declarations

Conflict of interest ZX is an editorial board member and TZ is an associate editor for *Bio-Design and Manufacturing*; they were not involved in the editorial review or the decision to publish this article. The authors declare that they have no known competing financial interests or personal relationships that could have appeared to influence the work reported in this paper.

Ethical approval All animal experiments were conducted in adherence to the guidelines of Tsinghua University, which is accredited by the Association for Assessment and Accreditation of Laboratory Animal Care International (AAALAC). All protocols were approved by the Institutional Animal Care and Use Committee (IACUC) of Tsinghua University (identification number: THU-LARC-2025-010).

Data availability The data that support the findings of this study are available from the corresponding authors upon reasonable request.

References

1. Small EM, Thatcher JE, Sutherland LB et al (2010) Myocardin-related transcription factor-A controls myofibroblast activation and fibrosis in response to myocardial infarction. Circ Res 107(2): 294–304. https://doi.org/10.1161/CIRCRESAHA.110.223172
2. Huang K, Ozpinar EW, Su T et al (2020) An off-the-shelf artificial cardiac patch improves cardiac repair after myocardial infarction in rats and pigs. Sci Transl Med 12(538):eaat9683. https://doi.org/10.1126/scitranslmed.aat9683
3. Contessotto P, Pandit A (2021) Therapies to prevent post-infarction remodelling: from repair to regeneration. Biomaterials 275:120906. https://doi.org/10.1016/j.biomaterials.2021.120906
4. Liu ZB, Tian YM, Wu BY et al (2025) Treating myocardial infarction with 3D-printed conductive myocardial patch fabricated from granular composite hydrogel. Int J Bioprint 11(2):234–248. https://doi.org/10.36922/ijb.6156
5. Yin Q, Zhu P, Liu W et al (2023) A conductive bioengineered cardiac patch for myocardial infarction treatment by improving tissue electrical integrity. Adv Healthc Mater 12:2201856. https://doi.org/10.1002/adhm.202201856
6. Jang J, Park HJ, Kim SW et al (2017) 3D printed complex tissue construct using stem cell-laden decellularized extracellular matrix bioinks for cardiac repair. Biomaterials 112:264–274. https://doi.org/10.1016/j.biomaterials.2016.10.026
7. Li M, Wu H, Yuan YH et al (2022) Recent fabrications and applications of cardiac patch in myocardial infarction treatment. VIEW 3:20200153. https://doi.org/10.1002/VIW.20200153
8. Lyu YN, Xie JH, Liu Y et al (2020) Injectable hyaluronic acid hydrogel loaded with functionalized human mesenchymal stem cell aggregates for repairing infarcted myocardium. ACS Biomater Sci Eng 6(12):6926–6937. https://doi.org/10.1021/acsbiomaterials.0c01344
9. Wang W, Chen JR, Li M et al (2019) Rebuilding postinfarcted cardiac functions by injecting TIIA@PDA nanoparticle-cross-linked ROS-sensitive hydrogels. ACS Appl Mater Interfaces 11(3):2880–2890. https://doi.org/10.1021/acsami.8b20158
10. Wu TL, Cui CY, Huang YT et al (2020) Coadministration of an adhesive conductive hydrogel patch and an injectable hydrogel to treat myocardial infarction. ACS Appl Mater Interfaces 12(2): 2039–2048. https://doi.org/10.1021/acsami.9b17907
11. Liang S, Zhang YY, Wang HB et al (2018) Paintable and rapidly bondable conductive hydrogels as therapeutic cardiac patches. Adv Mater 30(23):1704235. https://doi.org/10.1002/adma.201704235
12. Zhou RY, Yu JC, Gu Z et al (2022) Microneedle-mediated therapy for cardiovascular diseases. Drug Deliv Transl Res 12:472–483. https://doi.org/10.1007/s13346-021-01073-7
13. Lim S, Park TY, Jeon EY et al (2021) Double-layered adhesive microneedle bandage based on biofunctionalized mussel protein for cardiac tissue regeneration. Biomaterials 278:121171. https://doi.org/10.1016/j.biomaterials.2021.121171
14. Chen HT, Fan L, Peng NX et al (2022) Galunisertib-loaded gelatin methacryloyl hydrogel microneedle patch for cardiac repair after myocardial infarction. ACS Appl Mater Interfaces 14(36): 40491–40500. https://doi.org/10.1021/acsami.2c05352
15. Hu SQ, Zhu DS, Li ZH et al (2022) Detachable microneedle patches deliver mesenchymal stromal cell factor-loaded nanoparticles for cardiac repair. ACS Nano 16(10):15935–15945. https://doi.org/10.1021/acsnano.2c03060
16. Chen XR, Chen H, Zhu LY et al (2024) Nanoparticle-patch system for localized, effective, and sustained miRNA administration into infarcted myocardium to alleviate myocardial ischemia-reperfusion injury. ACS Nano 18(30):19470–19488. https://doi.org/10.1021/acsnano.3c08811
17. Tang JN, Wang JQ, Huang K et al (2018) Cardiac cell-integrated microneedle patch for treating myocardial infarction. Sci Adv 4(11):eaat9365.

https://doi.org/10.1126/sciadv.aat9365
18. Fang A, Wang YF, Guan NY et al (2023) Porous microneedle patch with sustained delivery of extracellular vesicles mitigates severe spinal cord injury. Nat Commun 14(1):4011. https://doi.org/10.1038/s41467-023-39745-2
19. Fang YC, Guo YH, Ji MK et al (2022) 3D printing of cell-laden microgel-based biphasic bioink with heterogeneous microenvironment for biomedical applications. Adv Funct Mater 32(13): 2109810. https://doi.org/10.1002/adfm.202109810
20. Zhou XH, Fang YC, Zhang T et al (2024) Retrospective: advances and opportunities of 3D bioprinting in China over three decades. Addit Manuf Front 3(4):200157. https://doi.org/10.1016/j.amf.2024.200157
21. Ding ZC, Liang ZM, Rong X et al (2024) Janus-structured microgel barrier with tissue adhesive and hemostatic characteristics for efficient prevention of postoperative adhesion. Small 20(50):2403753. https://doi.org/10.1002/smll.202403753
22. Zhang J, Luo XX, Liu JQ et al (2025) A "Janus" zwitterionic hydrogel patch for tissue repair and prevention of post-operative adhesions. Adv Healthc Mater 14(3):2404082. https://doi.org/10.1002/adhm.202404082
23. Liang QH, Chen SH, Hua SF et al (2025) Biomimetic versatile anisotropic, electroactive cellulose hydrogel scaffolds tailored from fern stem serving as nerve conduit and cardiac patch. Adv Sci 12(4):2400002. https://doi.org/10.1002/advs.202400002
24. Zou Y, Li L, Li Y et al (2021) Restoring cardiac functions after myocardial infarction-ischemia/reperfusion via an exosome anchoring conductive hydrogel. ACS Appl Mater Interfaces 13(48): 56892–56908. https://doi.org/10.1021/acsami.1c16481
25. DiStefano TJ, Vaso K, Panebianco CJ et al (2022) Hydrogel-embedded poly(lactic-co-glycolic acid) microspheres for the delivery of hMSC-derived exosomes to promote bioactive annulus fibrosus repair. Cartilage 13(3):19476035221113959. https://doi.org/10.1177/19476035221113959
26. Gan JJ, Zhang XX, Ma WJ et al (2022) Antibacterial, adhesive, and MSC exosomes encapsulated microneedles with spatiotemporal variation functions for diabetic wound healing. Nano Today 47:101630. https://doi.org/10.1016/j.nantod.2022.101630